Z. Kristallogr. **222** (2007) 650–655 / **DOI** 10.1524/zkri.2007.222.11.650

X-ray computed tomography in Zernike phase contrast mode at 8 keV with 50-nm resolution using Cu rotating anode X-ray source

Andrei Tkachuk*, Fred Duewer, Hongtao Cui, Michael Feser, Steve Wang and Wenbing Yun

Xradia, Inc. 5052 Commercial Circle, Concord, CA 94597, USA

Received May 30, 2007; accepted August 13, 2007

X-ray microscopy / Computed tomography / Fresnel zone plate / SOFC / Fuel cell / Nanotechnology

Abstract. High-resolution X-ray computed tomography (XCT) enables nondestructive 3D imaging of complex structures, regardless of their state of crystallinity. This work describes a sub-50 nm resolution XCT system operating at 8 keV in absorption and Zernike phase contrast modes based on a commercially available Cu rotating anode laboratory X-ray source. The system utilizes a high efficiency reflective capillary condenser lens and high-resolution Fresnel zone plates with an outermost zone width of 35 nm and 700 nm structure height resulting in a spatial resolution better than 50 nm currently. Imaging a fragment of the solid oxide fuel cells (SOFC) with 50 nm resolution is presented as an application example of the XCT technique in materials science and nanotechnology.

Introduction

Structure determination of crystalline materials is routinely performed by X-ray and neutron diffraction techniques capable of achieving atomic resolution. However, in the absence of long-range order, direct imaging techniques are required for structural analysis. Visible light or electron microscopy techniques are commonly employed and widely available. However, they may not be always applicable for nondestructive imaging if the specimen is either optically opaque to visible light or too thick to be penetrated by electrons. X-rays offer superior imaging resolution compared to visible light due to the short wavelength of X-rays. In general X-rays also have much higher penetrative power than electrons since they don't interact with matter as strongly as a charged particle.

Currently there are two successful approaches to high-resolution full field X-ray imaging: direct imaging which uses a high resolution Fresnel lens as the objective [1–3] and diffractive imaging that does not use a lens but requires coherent illumination currently only provided by synchrotron sources [4, 5]. In recent years, both imaging techniques have demonstrated rapidly improving resolution: 15 nm using the first approach [6] and sub-30 nm by the second approach [5]. While direct imaging requires a high-resolution X-ray lens similar to that of a standard optical microscope, it does not require a synchrotron source with high degree of coherence. Direct imaging also has the advantage of having immediate feedback of visualizing 2D projection images collected during the data acquisition rather than exclusively relying on post acquisition reconstruction algorithms to "see" the sample as in the case of diffractive imaging.

The X-ray computed tomography (XCT) is a direct-imaging technique that has been successfully used over two decades for biological imaging in the high contrast "water window" (284–560 eV) X-ray energy range [6, 7]. However, for semiconductor, materials science and nanotechnology applications significantly denser materials require more energetic X-rays to penetrate specimens tens or even hundreds of microns thick. For this purpose we developed a hard X-ray tomographic X-ray microscope based on a commercial X-ray generator using the Cr-K_α emission line (5.4 keV), which was commercialized in 2003 for semiconductor failure analysis as the primary application [1]. This system enables 3D tomographic imaging of Cu interconnects through up to 30 μm thick integrated circuit (IC) silicon dies. In order to increase the transmission in Si from 30 μm up to 100 μm, the operating energy has been changed to the Cu-K_α (8 keV) emission line [3]. In addition, a system that can be coupled with a synchrotron source operating at 7–18 keV has been introduced [2]. Since the absorption contrast diminishes rapidly with X-ray energy ($\sim 1/E^3$), we have equipped the XCT system with Zernike phase contrast optics that take advantage of the slower drop-off (1/E) of phase contrast with increasing X-ray energy.

In this paper we demonstrate the technical capabilities of the TXM to image complex porous structures of the solid oxide fuel cells (SOFC) [8] with 50 nm spatial resolution. Fuel cell devices convert chemical energy directly into electrical energy without combustion. Its immediate benefit is much higher energy conversion efficiency and the reduction of pollutants. SOFC, in particular, are able to utilize widely used hydrocarbon fuel to simultaneously generate thermal and electrical power with combined heat and power efficiency of over 80%. The electrochemical reactions occur in a narrow zone along the *three-phase*

* Correspondence author (e-mail: atkachuk@xradia.com)

boundary (TPB), where the cathode material, the solid electrolyte, and the gas are in contact. Better electrochemical performances are expected for components with higher TPB length per unit area. Much of SOFC research and development efforts are therefore focused on producing nano-porous structures with maximum TPB length as well as optimizing operating conditions that allow high performance and longevity. It is critical to be able to nondestructively image these nano-porous structures in 3D to study the size, distribution, and connectivity of the pores and channels. Furthermore, it is desirable to study the dynamic changes of these structures *in-situ* and while the device is in operation. In fact, utilizing synchrotron radiation sources, which have much higher brightness (throughput) and higher energy (X-ray transmission), will allow in-situ studies of the fuel cells at operating conditions. Xradia, Inc. has recently installed an X-ray microscope at Advanced Photon Source, Argonne National Laboratory at beamline ID-32 operating at X-ray energies up to 18 keV, which is sufficient to penetrate SOFC materials up to 1 mm thick.

Design and performance of full field X-ray microscope

Figure 1 shows schematically the main components of the tomographic X-ray microscope. The microscope is configured as a full-field transmission microscope much like a transmission electron microscope or a regular visible light microscope.

A commercial Cu X-ray rotating anode with ~100 μm diameter source size is employed to generate Cu-K_α emission line ($E = 8.05$ keV, wavelength $\lambda = 1.54$ Å). A reflective condenser optic with ellipsoidal surface figure refocuses the X-rays onto the sample. Compared to Fresnel zone plates as condenser optics, this reflective condenser has the advantage of having a much higher numerical aperture matching the one of the imaging zone plate and a much higher focusing efficiency (>90%). The sample is located on a high-precision rotation stage that allows acquiring 2-D projection images from +/− 90 degree range of rotation angles. The key element, the objective, is a Fresnel zone plate. Fresnel zone plates are diffractive optical elements (see Fig. 4), which focus X-rays by means of diffraction not refraction [9]. The Fresnel zone plate objective creates a magnified image of the sample on a high-resolution X-ray detector as shown in Fig. 2. For a compact microscope it is advantageous to employ a very high spatial resolution X-ray detector in order to minimize the sample to detector imaging distance while maintaining a high magnification.

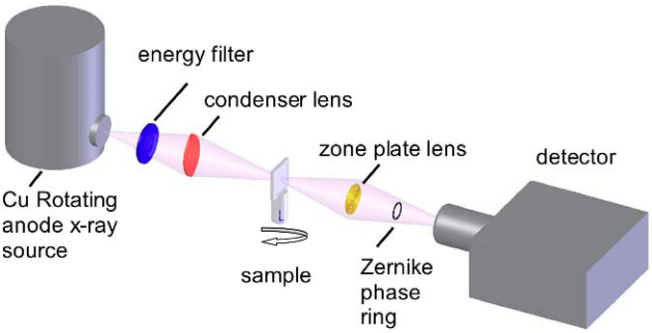

Fig. 1. Illustration of the zone-plate based X-ray microscope operating in Zernike phase contrast mode. The condenser lens is a reflective ellipsoidal capillary with ~90% reflection efficiency, which refocuses ~100 μm X-ray source spot from the Cu rotating anode onto the sample. A Fresnel lens zone plate objective lens with 35 nm outermost zone width and 700 nm zone height magnifies the image onto high resolution X-ray detector. The Zernike phase ring is positioned near the back focal plane of the zone plate lens to phase shift the X-rays not scattered by the sample by 3π/2 (negative phase contrast).

In addition, it is very important to use a detector with very high quantum efficiency to use all X-ray photons in the detection process. We have developed a detection system with >90% quantum detection efficiency and effective pixel size better than 2 μm based on a scintillation screen coupled to a CCD detector. The Rayleigh resolution δ of a X-ray microscope is a function of the outermost zone width Δr_n of the objective zone plate:

$$\delta = 1.22\,\Delta r_n\,. \tag{1}$$

This formula is strictly only valid for coherent illumination (parallel light), and better resolution is routinely obtained using incoherent illumination (illumination from a range of angles) [11]. Using the simple Rayleigh formalism, the theoretical resolution of the objective zone plate with $\Delta r_n = 35$ nm is computed to be $\delta = 42.7$ nm using Eq. 1. Note that the resolution of the zone-plate based X-ray microscope is independent of X-ray source spot size and ultimately limited by the outermost zone width of the zone plate (finer zones give higher resolution). Figure 3 depicts the transmission image of Au resolution test pattern 600 nm high (Au structure appears with dark contrast). The width of the Au tips inside the most inner circle is 50 nm.

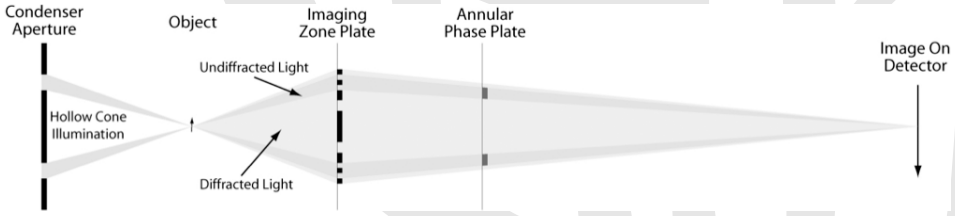

Fig. 2. Imaging geometry: capillary reflective condenser produces hollow cone illumination designed to nearly match the numeric aperture of the imaging zone plate. Annular phase ring is positioned at the back focal plane of the imaging zone plate to intercept the undiffracted X-ray light (darker shade of grey). Diameter and width of the phase ring were chosen to intercept all of the undiffracted light. The phase ring was manufactured with thickness required to shift the phase of the undiffracted light by 3π/2 +/− π/8 (see Fig. 5).

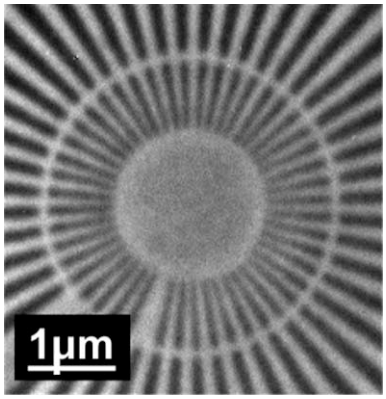

Fig. 3. Transmission image of 600 nm thick Au pattern taken with laboratory X-ray microscope operating at 8 keV in Zernike phase contrast mode using objective zone plate with 35 nm outermost zone width. The line width of the dark Au tips inside the most inner circle is 50 nm. As a consequence, the resolution of the X-ray microscope is inherently coupled to the progress of the fabrication technology of Fresnel zone plates. While it is relatively simple to pattern high-resolution structures using electron beam lithography, it is very challenging to fabricate these fine features very tall, which is needed in X-ray focusing to have sufficient focusing efficiency. Examples of the zone plates with high aspect ratios manufactured by Xradia, Inc are shown in Fig. 4.

For implementation of Zernike phase contrast a transmissive phase ring is added in the back focal plane of the objective zone plate as shown in Fig. 2 [10]. The phase ring is fabricated out of gold and has a thickness designed to produce a phase shift of $3\pi/2$ of the X-ray beam not diffracted by the sample. This phase shift produces negative phase contrast, i.e. features with net positive phase shift appear dark. The phase shifted undiffracted light interferes with un-shifted diffracted by the sample light, which produces phase contrast boost in the detector plane. The diameter and width of the annular phase ring was carefully selected to assure that all of the undiffracted condenser light is intercepted by the phase ring width. The plot of required phase ring thickness as a function of X-ray energy is shown in Fig. 5, which shows that ~2.5 µm Au thickness is required at 8 keV.

One big advantage of using 8 keV X-rays for imaging is that the working distance (distance between sample and objective) is quite large, which originates in the proportionality to X-ray energy E of the focal length f of a zone plate:

$$f = \frac{D\,\Delta r_n}{\lambda}\,, \tag{2}$$

where D is the diameter of the Fresnel zone plate objective. As an example, the working distance of the microscope operating at 8 keV with a zone plate of diameter <100 µm can be greater than 20 mm, which is 40 times more than typical working distances for "water-window" soft X-ray microscopes (typically $\ll$1 mm working distance).

The price to pay for a long working distance L_1 is that the imaging distance L_2 can be quite large since the X-ray magnification M of the microscope has to be quite large due to quite poor spatial resolution of area X-ray detectors. The geometric magnification is given as:

$$M = \frac{L_2}{L_1}\,. \tag{3}$$

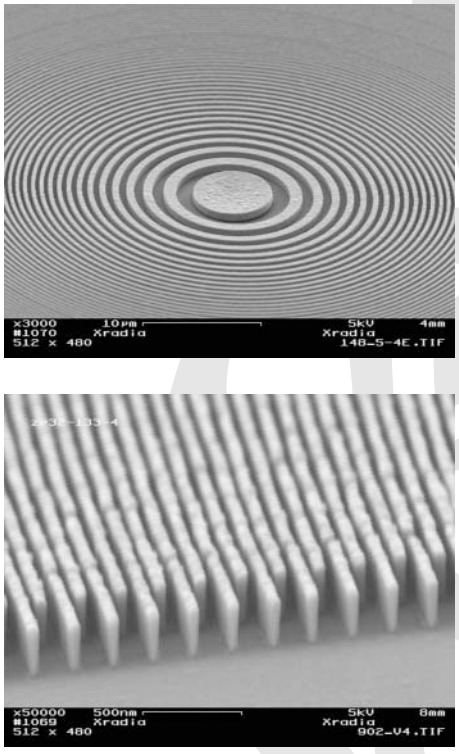

Fig. 4. SEM images: (**a**) central portion of the Au Fresnel zone plate with 50 nm outermost zone width. The width of the concentric circles (zones) diminishes outward from the center until the outermost zone width becomes 50 nm; (**b**) 50 nm outermost zone width test structures with 450 nm zone height. Aspect ratios up to 1:30 have been achieved at Xradia, Inc. by permanently bonding two zone plates on top of each other with an alignment accuracy of $^1/_3$ of the outermost zone width. (zone plates were manufactured by Xradia, Inc.).

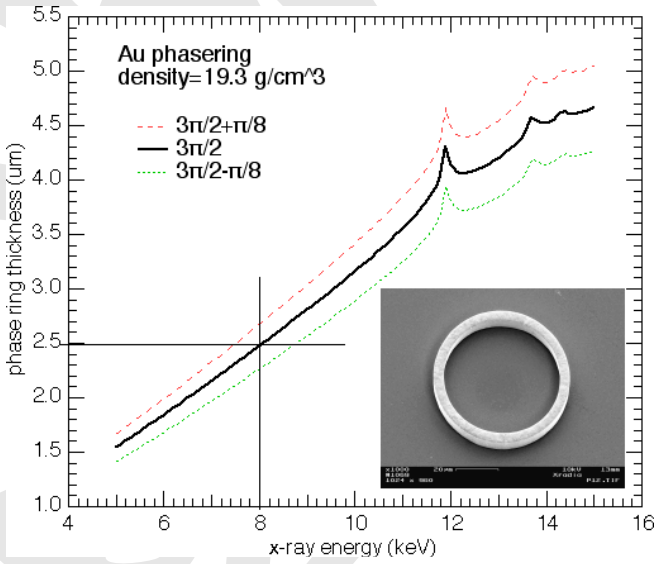

Fig. 5. Thickness of the Au phase ring plotted as a function of X-ray energy required to produce a phase shift $3\pi/2$ (solid curve). The inset shows SEM image of the Au phase ring structure on top of silicon nitride window, which is transparent to X-rays. The targeted phase ring thickness was selected to produce $3\pi/2$ +/− $\pi/8$ phase shift (dashed curves) for optimal negative Zernike phase contrast at 8 keV.

L_2 and L_1 are distances that satisfy the well-known thin lens imaging condition

$$\frac{1}{f} = \frac{1}{L_1} + \frac{1}{L_2} . \quad (4)$$

To obtain an imaging resolution of 50 nm, the sample pixel size has to be oversampled by a factor of ~2.5, leading to a physical pixel size of 20 nm in the sample plane. Using the high resolution X-ray imaging detector with ~0.65 μm effective pixel size the required X-ray magnification is $M \sim 32$ and therefore the image distance L_2 gets close to 600 mm. Higher geometrical magnification $M \sim 50$ can be achieved by increasing L_2 up to ~1 m at the expense of the field of view and imaging throughput.

A second big advantage of a hard X-ray microscope over a "water-window" soft X-ray microscope is the long depth of focus, which is needed for tomography. The requirement for computed tomography based on back-projection is that the whole reconstructed volume has to be within the depth of focus of the microscope. Quantitatively, the depth of focus *DOF* is given by:

$$DOF = \pm \frac{\lambda}{2NA^2} = \pm \frac{2\Delta r_n^2}{\lambda} , \quad (5)$$

where *NA* is the numerical aperture of the zone plate defined by:

$$NA = \frac{\lambda}{2\Delta r_n} \quad (6)$$

where λ is the X-ray wavelength and Δr_n the outermost zone width of the objective zone plate. For example for 8 keV X-rays ($\lambda = 0.154$ nm) and a zone plate with 35 nm outermost zone width, the corresponding numerical aperture is 2.2 mrad, and *DOF* is approximately 32 μm, which is very comfortable for high-resolution tomography. In contrast using the same outermost zone width zone plate of 35 nm with soft X-rays, *e.g.* 3 nm wavelength, the *DOF* is severely reduced to less than 2 μm, which clearly poses a problem for high-resolution tomography of larger volumes. SOFC fragments with thickness very close to the 32 μm *DOF* still have reasonable X-ray transmission for imaging at 8 keV. In contrast, soft X-rays with energies <1 keV can not penetrate even 1 μm of SOFC ceramic typically composed of a solid yttria stabilized zirconia (YSZ) electrolyte and a porous nickel YSZ (Ni-YSZ) anode.

Experimental results

Large $DOF = 32$ μm, large working distances of $L_1 \sim 20$ mm and reasonable X-ray transmission at 8 keV through up to 32 μm of material are very well suited for high-resolution tomographic 3D imaging of macroscopic dense objects, such as SOFC. The sample imaged with the XCT system was the tip of a piece broken off from a hollow tubular SOFC, with a solid YSZ electrolyte shell and a much thicker porous Ni-YSZ anode layer on the inside [8]. Raw data is shown in Fig. 6 as it appears on the computer screen of the microscope. Only two selected projections are shown in Fig. 6 out of 181 collected 2D projections. Each projection is imaged by high resolution CCD detector while rotating the sample every degree from −90 to +90 degrees as schematically depicted in Fig. 1. Data collection is fully automated with 5 min/projection exposure time in order to obtain the data with good single to noise ratio. Image intensity in Fig. 6 is proportional to density and thickness of the material, *e.g.* denser and/or thicker materials appear darker on the image. Since atomic density of the solid and porous material are very similar, solid YSZ electrolyte appears darker on the left image because of greater projected thickness the X-rays had to penetrate at this particular imaging angle.

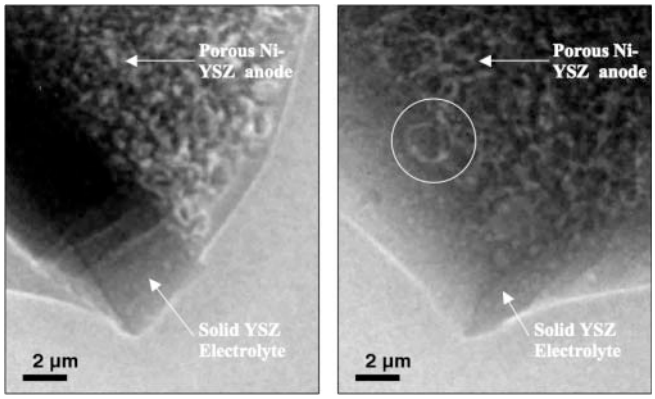

Fig. 6. Raw data produced by X-ray microscope operating at 8 keV in Zernike phase contrast mode. 181 projections (only two are shown) were taken every degree from −90 to +90 angular range. The gray level image intensity is such that the denser and/or thicker the material the darker it appears on the image. Solid YSZ electrolyte and porous Ni-YSZ anode are clearly distinguished on the images. The circled feature on the right image will be used as a reference in subsequent figures of the reconstructed volume. Data acquisition time was 5 min per 2D projection.

A computed tomography was performed to reconstruct a 3D volume of the object from a series of 181 2D projections by applying parallel beam filtered back projection (FBP) algorithm [12] using internally developed software which controls all the functions of the microscope. Reconstructing the exact phase image from Zernicke phase contrast data can be very difficult and even lead to confusing results. Therefore, we find it practical to simply do normal FBP with the caveat that the viewer should be aware of artifacts that can arise from this procedure. Typical imaging artifacts are bright halos, which are especially pronounced around the edges of the lower spatial frequency features in Fig. 6. These halos often appear in the FBP reconstructions, however can be often distinguished from the real features. The bright halos often overlap around the features having high spatial frequencies, which produces relatively uniform backround not obscuring the real features as seen in Fig. 3 for known Au lithography pattern. Appearance of the edge halos was suppressed by controlling the threshold in the visualization software as shown in Figs. 7 and 8.

The full Xradia software suite [13] consists of three separate programs: TXM Controller, 3D Reconstructor and 3D Viewer integrated into a complete package. Output of one of the programs becomes an input of the next one during data acquisition and analysis procedure. TXM Controller coordinates all of the data acquisition, tomographic

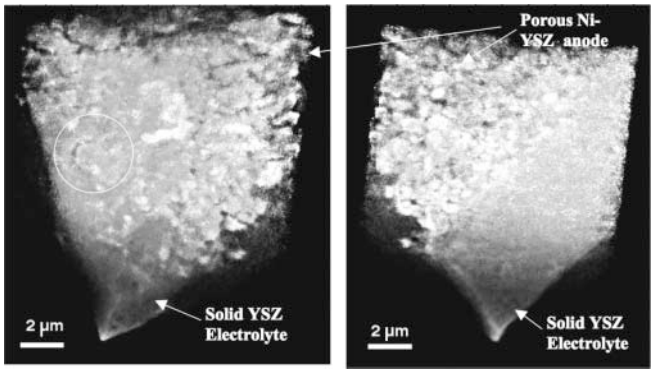

Fig. 7. Reconstructed volume of the SOFC reconstructed from 181 projections (see Fig. 6) taken between −90 to 90 degrees angular range. Note that the contrast is reversed compared to Fig. 6, *e.g.* the SOFC material appears in bright color against black background (air). Barely visible circled feature is the one referenced in Fig. 6 and Fig. 8.

data collection and 2D processing functions of the microscope. TXM Controller software performs fully automated tomographic data acquisition. 2D projections collected during sample rotation are processed by 3D Reconstructor module. Because of the small $\sim 20 \times 20$ μm field of view and low divergence of the collected X-rays (NA of the objective zone plate is ~3 mrad) fast parallel beam reconstruction was applied instead of slower and more involved cone beam reconstruction. Hardware accelerated software completes reconstruction of $512 \times 512 \times 512$ pixel volume on a modern 2.7 GHz single processor PC in under 90 sec. The reconstructed volume can be further viewed and manipulated using the 3D Viewer module of the software suite. Snapshots of the reconstructed 3D volume of the SOFC fragment at two different rotation angles are shown in Fig. 7.

The reconstructed 3D volume of the SOFC fragment subsequently can be "virtually delayered" (commonly known as tomographic sectioning) in any direction for on-screen viewing or exported for subsequent data analysis [14]. Two sections extracted from the 3D volume in Fig. 7 separated by ~1 μm are shown in Fig. 8. Tomographic sectioning is very valuable when the structural identity of the specimen must remain intact. Figure 5 clearly depicts the Solid YSZ electrolyte – Ni YSZ anode interface, as well as nano-porosity and tortuosity, which are important for understanding the mechanisms responsible for optimizing operating conditions of SOFCs that allow high performance and longevity. The ability to image these nano-porous structures in 3D to study the size, distribution, and connectivity of the pores and channels is critical in enabling SOFC technology. Detailed analysis and modeling based on the results of this work are currently underway and will be presented elsewhere [14].

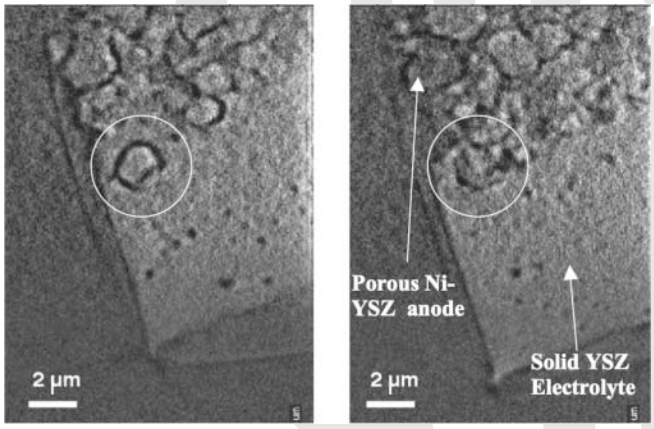

Fig. 8. Examples of two tomogaphic sections ~1 μm apart extracted from the reconstructed 3D volume shown in Fig. 7. Circular region used as reference in Fig. 6 and Fig. 7 is shown. Sub 100 nm pores (dark dots) are visible inside the solid YSZ electrolyte wall. Porosity and channels inside the porous Ni-YSZ anode are also clearly visible together with PTB interface separating solid and porous regions.

Conclusions and outlook

We have demonstrated 50 nm resolution tomographic 3D imaging of $\sim 20 \times 20 \times 20$ μm fragments of a tubular solid oxide fuel cells (SOFC) with a hard X-ray microscope based on a laboratory X-ray source operating at 8 keV X-ray energy in Zernike phase contrast mode. The practicality of the X-ray microscope is based on our development of high performance, high efficiency X-ray optical components, namely the X-ray capillary condenser lens, the X-ray objective zone plate, and the X-ray detector. Tomographic sectioning and segmentation of the reconstructed data offers a completely nondestructive way to inspect multiple layers from the 3D reconstructed volume for visualization and subsequent data analysis and modeling. Detailed analysis and modeling of the size, distribution, and connectivity of the pores and channels, which are important for SOFC performance and longevity will be published elsewhere [14]. In the future, the continued advancement in zone plate resolution and efficiency in the hard X-ray energy range promises even higher throughput and spatial resolution, since the resolution of the X-ray lens currently is only limited by manufacturing capabilities. The development of novel laboratory X-ray sources and the utilization of high brightness synchrotron sources will open new opportunities for faster, higher resolution X-ray microscopy. It is expected that high resolution XCT using hard X-rays will proliferate into many areas of R&D and industrial applications as a standard nondestructive microscopy technique that bridges the gap between visible light and electron microscopy.

Acknowledgments. We thank John R. Izzo Jr and Wilson K. S. Chiu (Department of Mechanical Engineering, University of Connecticut) for providing the SOFC samples and stimulating discussions. SOFC anode samples are manufactured by Adaptive Materials Inc. (Ann Arbor, MI).

References

[1] Wang, S.; Duewer, F.; Kamath, S.; Kelley, C.; Lyon, A.; Nill, K.; Scott, D.; Trapp, D.; Yun, W.: A transmission x-ray microscope (TXM) for nondestructive 3D imaging of IC's at sub 100-nm Resolution. Proceedings of 28th ISTFA Conference, Phoenix, AZ (2002) 227–233.

[2] Yin, G.-C.; Tang, M.-T.; Song, Y.-F.; Chen, F.-R.; Liang, K. S.; Duewer, F.; Yun, W.; Ko, C.-H.; Shieh, H.-P. D.: Energy-tunable transmission X-ray microscope for differential contrast imaging with near 60 nm resolution tomography. Appl. Phys. Lett. **88** (2006) 241115.

[3] Tkachuk, A.; Feser, M.; Cui, H.; Duewer, F.; Chang, H.; Yun, W.: High-resolution X-ray tomography using laboratory sources. Proceedings of SPIE **6318**, 63181D (2006)
[4] Sayre, D.; Chapman, H. N.: X-ray Microscopy. Acta Cryst. **51** (1995) 237–252.
[5] Miao, J.; Hodgson, K. O.; Ishikawa, T.; Larabell, C. A.; LeGros, M. A.; Nishino, Y.: Imaging whole Escherichia coli bacteria by using single-particle x-ray diffraction. Proc. Natl. Acad. Sci. USA **100** (2003) 110.
[6] Chao, W.; Harteneck, B. D.; Liddle, J. A.; Anderson, E. H.; Attwood, D. T.: Soft X-ray microscopy at a spatial resolution better than 15 nm. Nature **435** (2005) 1210–1213.
[7] Rudolph, D.; Schmahl, G.; Niemann, B.: Amplitude and phase contrast in x-ray microscopy. Modern Microscopies. New York, Plenum, 59–67 (1990).
[8] Wilson, J. R.; Kobsiriphat, W.; Mendoza, R.; Chen, H.; Hiller, J. M.; Miller, D. J.; Thornton, K.; Voorhees, P. W.; Adler, S. B.; Barnett, S. A.: Three-dimensional reconstruction of a solid-oxide fuel-cell anode. Nature Materials Letters (2006).
[9] Young, M.: Zone plates and their aberrations. J. Optical Society of America **62**(8) (1972) 972–976.
[10] Zernike, F.: Das Phasenkontrastverfahren bei der mikroskopischen Beobachtung. Zeitschrift für technische Physik **36** (1935) 848–851.
[11] Schneider, G.: Cryo X-ray microscopy with high spatial resolution in amplitude and phase contrast. Ultramicroscopy, **75** (1998) 85–104.
[12] Born, M.; Wolf, E.: Principles of Optics. Cambridge University Press, p. 217–227, (1999).
[13] Xradia, Inc.: http://www.xradia.com.
[14] Izzo Jr., J. R.; Joshi, A. S.; Grew, K. N.; Chiu, W. K. S.; Tkachuk, A.; Wang, S.; Yun, W.: X-ray computed tomography and analysis of solid oxide fuel cell anodes at 50 nm resolution. Nature Materials, submitted.